

Thermoelectric Properties and Electronic Structure of the Cage Compounds $A_2BaCu_8Te_{10}$ ($A = K, Rb, Cs$): Systems with Low Thermal Conductivity

Rhonda Patschke,[†] Xiang Zhang,[†] David Singh,[‡] Jon Schindler,[§]
 Carl R. Kannewurf,[§] Nathan Lowhorn,^{||} Terry Tritt,^{||} George S. Nolas,[⊥] and
 Mercouri G. Kanatzidis^{*,†}

Department of Chemistry and Center for Fundamental Materials Research,
 Michigan State University, East Lansing, Michigan 48824, Complex Systems Theory Branch,
 Naval Research Laboratory, Washington, DC 20375, Department of Electrical Engineering and
 Computer Science, Northwestern University, Evanston, Illinois 60208, Department of Physics
 and Astronomy, Clemson University, Clemson, South Carolina 29634, and R&D Division,
 Marlow Industries Inc., 10451 Vista Park Road, Dallas, Texas 75238

Received May 11, 2000. Revised Manuscript Received November 9, 2000

The anisotropic, two-dimensional structure of the compounds $A_2BaCu_8Te_{10}$ ($A = K, Rb, Cs$) fits the description of a “phonon glass electron crystal” (PGEC) which is proposed to be a desirable feature of a good thermoelectric material. It contains Cu_8Te_{12} pentagonal dodecahedral cages filled with Ba^{2+} atoms. These cages are fused together to make $[BaCu_8Te_{10}]^{2-}$ slabs which are separated by alkali metal atoms. Electronic band structure calculations on $Cs_2BaCu_8Te_{10}$ at the density functional theory (DFT) level show a complex electronic structure near the Fermi level. The Fermi level falls in a deep valley in the density of states, a pseudogap in which very few states exist. Heat capacity, magnetic susceptibility, and infrared absorption measurements, however, suggest that these materials are narrow gap semiconductors with a band gap of approximately 0.28 eV. Electrical conductivity, thermopower, and thermal conductivity measured on polycrystalline ingots are reported, and the results are discussed in the context of the calculated electronic structure and the PGEC model. It is suggested that while the PGEC aspects of the compounds may have an effect on the thermoelectric properties, they are not the dominant factor responsible for the very low thermal conductivity of these materials.

Introduction

Currently, there is a strong impetus toward identifying thermoelectric materials with $ZT > 1$.^{1,2} The challenge in these efforts lies in achieving simultaneously high electrical conductivity, high thermoelectric power, and low thermal conductivity in the same solid. These properties define the thermoelectric figure of merit $ZT = (S^2\sigma/\kappa)T$, where S is the thermopower, σ is the electrical conductivity, κ is the thermal conductivity, and

T is the absolute temperature. The first two quantities are determined by the details of the electronic structure and scattering of charge carriers (electrons or holes) and thus are not independently controllable parameters. The thermal conductivity, κ , has a contribution from lattice vibrations, κ_l , as well as from charge carriers, κ_e ; thus, $\kappa = \kappa_e + \kappa_l$. One way to increase ZT is to minimize κ_l while retaining good electrical and thermopower properties. While there are several approaches to minimizing κ_l , the most intriguing is the one associated with the concept of “phonon glass electron crystal” (PGEC) which was introduced by Slack as the limiting characteristic for a superior thermoelectric.³ A PGEC material features cages (or tunnels) in its crystal structure inside which reside atoms small enough to “rattle”; i.e., create dynamic disorder. This situation produces a phonon damping effect which results in a reduction of the solid's lattice thermal conductivity. If the atomic orbitals of the “rattling” ions do not get substantially involved in the

* To whom correspondence should be addressed.

[†] Michigan State University.

[‡] Naval Research Laboratory.

[§] Northwestern University.

^{||} Clemson University.

[⊥] Marlow Industries Inc.

(1) (a) *Thermoelectric Materials 1998-The Next Generation Materials for Small-Scale Refrigeration and Power Generation Applications*, Material Research Society Symposium Proceedings 545; Tritt, T. M., Kanatzidis, M. G., Mahan, G. D., Lyon H. B., Eds.; MRS: Pittsburgh, PA, 1988. (b) *Thermoelectric Materials-New Directions and Approaches*, Material Research Society Symposium Proceedings 478; Tritt, T. M., Kanatzidis, M. G., Lyon, H. B., Mahan, G. D., Eds.; MRS: Pittsburgh, PA, 1997.

(2) (a) Chung, D.-Y.; Iordanidis, L.; Choi, K.-S.; Kanatzidis, M. G. *Bull. Kor. Chem. Soc.* **1998**, *19*, 1283–1293. (b) Kanatzidis, M. G.; DiSalvo, F. J. *Thermoelectric Materials: Solid State Synthesis*. *Naval Res. Rev.* **1996**, *68* (4), 14. (b) Kanatzidis, M. G. In *Semiconductors and Semimetals*; Tritt, T., Ed.; Academic Press: New York, 2000.

(3) (a) Slack, G. A. *New Materials and Performance Limits for Thermoelectric Cooling*. In *CRC Handbook of Thermoelectrics*; Rowe, D. M., Ed.; CRC Press: Boca Raton, FL, 1995; pp 407–440. (b) Slack, G. A. In *Thermoelectric Materials-New Directions and Approaches*, Material Research Society Symposium Proceedings 478; Tritt, T. M., Kanatzidis, M. G., Lyon, H. B., Mahan, G. D., Eds.; MRS: Pittsburgh, PA, 1997; p 47.

electronic structure near the Fermi level, the mobility of carriers is not likely to be substantially affected, thus not degrading potentially high electrical conductivity or thermopower.

Earlier, we reported on $A_2BaCu_8Te_{10}$ ($A = K, Rb, Cs$), a class of materials that possesses an anisotropic two-dimensional structure with Cu_8Te_{12} pentagonal dodecahedral cages.⁴ In this sense these compounds are related to those of the clathrates,⁵ but formally they do not belong to this class. These cages are linked together to produce infinite $[BaCu_8Te_{10}]^{2-}$ slabs. The alkali metal ions are located between the slabs, and on the basis of their atomic displacement parameters (ADPs), undergo substantial thermal motion in the interslab space.⁴ It is interesting to note that the Ba^{2+} ions encapsulated in the Cu_8Te_{12} cages hardly undergo any "rattling" motion. It is the A^+ atoms that undergo such motion potentially scattering acoustic phonons. Because the structure of $A_2BaCu_8Te_{10}$ contains characteristics that fit the description for a PGEC candidate thermoelectric material, we decided to take a closer look at the thermal conductivity, its thermoelectric properties, and the details of its electronic band structure. The narrow energy gap in these materials was probed with a variety of experimental techniques such as heat capacity, magnetic susceptibility, and infrared absorption measurements. The results are discussed in the context of the electronic structure and the PGEC concept. Here, we demonstrate that the materials combine both low thermal conductivity and high electrical conductivity and therefore are viable for systematic thermoelectric investigations.

Experimental Section

Synthesis. Single crystals of $Rb_2BaCu_8Te_{10}$ and $Cs_2BaCu_8Te_{10}$ were obtained as described previously.⁴ Polycrystalline ingots of $Rb_2BaCu_8Te_{10}$ and $Cs_2BaCu_8Te_{10}$ were prepared with a different method described here for the first time. A polycrystalline powder was first synthesized by heating a mixture of Rb_2Te or Cs_2Te (1 mmol), $BaTe$ (1 mmol), Cu (8 mmol), and Te (8 mmol) in a computer-controlled furnace to 520 °C in 12 h, isotherming at this temperature for 4–7 h, and quickly cooling to room temperature in 5 h. The polycrystalline powder sample is then placed in a long silica tube with a diameter of 5 mm and flame sealed. The sealed tube is placed into a gentle flame to melt the compound and immediately quenched to liquid-nitrogen temperatures. This liquid-nitrogen quenching process helps avoid the formation of vacuum pockets inside the ingot. The $K_2BaCu_8Te_{10}$ can be prepared in a similar way.

Dense, polycrystalline specimens for thermal conductivity measurements were prepared as follows: The crystals were ground to fine powders and hot pressed inside a graphite die at 280 °C and 21 500 lb/in.² for 3 h in an argon atmosphere. The resulting pellets had a density of 5.73 g/cm³ (Rb sample) and 5.94 g/cm³ (Cs sample), or >96% of theoretical density. Samples were cut from these pellets to dimensions 10 mm × 2 mm × 2 mm by a wire saw using 50 μm tungsten wire to ensure damage-free samples.

Physical Measurements. Electronic Transport Measurements. *Ingot Samples.* Polycrystalline ingot samples with typical sizes of 10 mm × 2 mm × 3 mm were cut from an ingot with a high-speed diamond saw. The ends of the samples were Ni plated and then were soldered to Cu blocks which had 0.003 in. Au–Fe (0.07 at. %) vs chromel thermocouples embedded in the Cu blocks to make the ΔT measurements. Cu lead wires were also soldered to these Cu blocks with one pair to serve as the current leads for the resistance measurements and another pair to serve as voltage leads (V_{TEP}) for the thermopower measurements. A pair of Au leads (V_R) were attached to the sample inside the current leads to measure the sample voltage for the resistance measurements. The sample voltages (V_{TEP} and V_R) as well as the thermocouple voltage (V_{TC}) were measured with a Keithley 2001 multivoltmeter. The Au–Fe vs chromel thermocouples provide adequate sensitivity even at the lower temperatures ($T \approx 4$ K). The temperature of the sample is determined using a Lake Shore calibrated Cernox sensor. We performed standard four-probe resistance measurements on all our samples. The resistance of the sample was obtained by a dc method of reversing the current (Keithley 2400) at each temperature and measuring the sample voltage and then taking an average to subtract the thermal voltages. Typical sample currents were 5–50 mA. All data was taken using high-speed computer data acquisition software and instrumentation.

The thermopower was measured in two different ways. First a standard V_{TEP} vs ΔT curve was taken at several temperatures with the gradient on the sample being swept from $-\Delta T$ to $+\Delta T$ with $\Delta T = 2$ –5% of the absolute temperature, T . The slope was calculated and the Au lead contribution subtracted thus giving the absolute thermopower of the material. We use this method to check at several temperatures our more typical method. In the latter method, a ΔT of 2–5% T was established across the sample and the resistance and thermopower were measured at essentially the same time, as discussed above. The temperature of the sample was slowly lowered using a variable-temperature dewar from $T \sim 300$ K to $T \sim 4$ K over a period of 14–16 h, and the resistance and thermopower were monitored as a function of temperature.

Single-Crystal Samples. Dc electrical conductivity and thermopower measurements were made on single crystals of the compounds. Conductivity measurements were performed in the usual four-probe geometry with 60- and 25-μm diameter gold wires used for the current and voltage electrodes, respectively. Measurements of the sample cross-sectional area and voltage probe separation were made with a calibrated binocular microscope. Conductivity data were obtained with the computer-automated system described elsewhere.⁶ Thermoelectric power measurements were made by using a slow-ac technique⁷ with 60-μm gold wires used to support and conduct heat to the sample, as well as to measure the voltage across the sample resulting from the applied temperature gradient. In both measurements, the gold electrodes were held in place on the sample with a conductive gold paste. Mounted samples were placed under vacuum (10^{-3} Torr) and heated to 320 K for 2–4 h to cure the gold contacts. For a variable-temperature run, data (conductivity or thermopower) were acquired during sample warming. The average temperature drift rate during an experiment was kept below 0.3 K/min. Multiple variable-temperature runs were carried out for each sample to ensure reproducibility and stability. At a given temperature, reproducibility was within $\pm 5\%$.

Thermoelectric power measurements done by the slow-ac technique require the production of a slowly varying periodic temperature gradient across the samples and measuring the resulting sample voltage. Samples were suspended between quartz block heaters by 60-μm gold wires thermally grounded to the blocks with GE 7031 varnish. The magnitude of the applied temperature gradient was generally 1.0 K. Smaller

(4) Zhang, X.; Park, Y.; Hogan, T.; Schindler, J. L.; Kannewurf, C. R.; Seong, S.; Albright T.; Kanatzidis, M. G. *J. Am. Chem. Soc.* **1995**, *117*, 10300–10310.

(5) (a) Nolas, G. S.; Weakley, T. J. R.; Cohn, J. L.; Sharma, R. *Phys. Rev. B* **2000**, *61*, 3845–3850. (b) Nolas, G. S.; Weakley, T. J. R.; Cohn, J. L. *Chem. Mater.* **1999**, *11*, 2470–2473. (c) Nolas, G. S.; Cohn, J. L.; Slack, G. A.; Schujman, S. B. *Appl. Phys. Lett.* **1998**, *78*, 178–180. (d) Cross, C.; Pouchard, M.; Hagenmuller, P.; *J. Solid State Chem.* **1970**, *2*, 570–581.

(6) Lyding, J. W.; Marcy, H. O.; Marks, T. J.; Kannewurf, C. R. *IEEE Trans. Instrum. Meas.* **1988**, *37*, 76–80.

(7) Marcy, H. O.; Marks, T. J.; Kannewurf, C. R. *IEEE Trans. Instrum. Meas.* **1990**, *39*, 756–760.

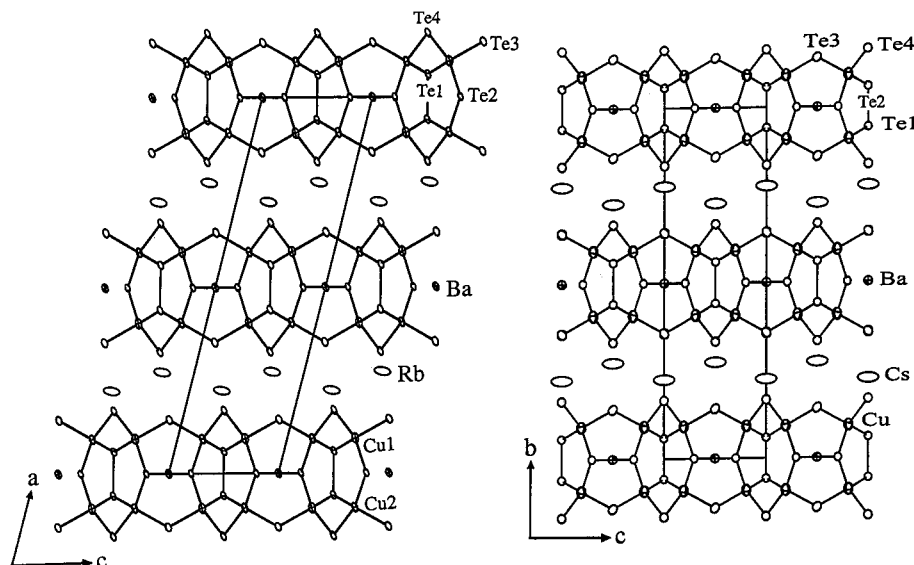


Figure 1. ORTEP representation of (left) the monoclinic crystal structure of Rb₂BaCu₈Te₁₀ (90% probability ellipsoids). The ellipses with octant shading represent Ba atoms, the crossed ellipses represent Cu atoms, and the large open ellipses represent Rb and Te atoms. (right) The Cs analogue has a similar structure; only the *a*- and *b*-axes are orthogonal.

temperature gradients gave essentially the same results but with somewhat lower sensitivity.

Thermal Conductivity. Steady-state thermal conductivity measurements were performed in a radiation-shielded vacuum probe with the heat flow measured along the longest axis. Heat losses via conduction through the lead wires and radiation were determined in separate experiments and the data corrected accordingly. These corrections were approximately 15% at room temperature and less at lower temperatures.

Heat Capacity. The heat capacity of Rb₂BaCu₈Te₁₀ was measured as a function of temperature, from 350 to 2 K, with a Quantum Design Physical Property Measurement System (PPMS). The sample platform base is suspended by fine wire on the heat capacity puck and contains its own temperature sensor and heater mounted under the base. A background file of the base platform and grease was measured, and the heat capacity measurement was obtained by subtracting out this background. The sample (mass = 5–50 mg) was mounted on the base with thermal grease for good thermal contact between the sample and the base platform. The PPMS uses a relaxation method to obtain the heat capacity of the sample or the background, where a ΔT is established between the sample and the base temperature. The heater is then turned off, and a relaxation curve is taken to determine the relaxation time. Typically, two records were taken at each temperature and averaged to determine the sample's heat capacity. The PPMS software has data fitting programs for the relaxation curves to extract the heat capacity at specific temperatures. The Debye temperature, Θ_D , and the electronic parameter, γ , were determined from the heat capacity vs temperature curves. Typically, two data sets were taken for each sample, one over a broad range of temperature and one focused in the low-temperature ($T < \Theta_D/50$) region. This enables the collection of a large density of data points which permits the accurate determination of the necessary information.

Magnetic Susceptibility. The magnetic response of Rb₂BaCu₈Te₁₀ was measured over the range of 2–300 K using an MPMS Quantum Design SQUID magnetometer. The sample was ground to a fine powder to minimize anisotropic effects, and corrections for the diamagnetism of the compound and the PVC sample container were applied. Magnetic susceptibility as a function of field strength (at a constant temperature of 300 K) was first investigated to determine if the samples experienced saturation of their magnetic signal. The magnetization increased linearly with increasing field over the range investigated (0–10 000 G). The subsequent temperature-dependent study was performed at 3000 G.

Infrared Absorption. Optical diffuse reflectance measurements were made on a finely ground sample at room temperature. The spectrum was recorded in the mid-IR region (6000–400 cm⁻¹) with a Nicolet MAGNA-IR 750 spectrometer equipped with a collector diffuse reflectance of Spectra-Tech Inc. The measurement of diffuse reflectivity can be used to determine the band gap. Absorption (α/S) data were calculated from the reflectance data using the Kubelka–Munk function.⁸ The band gap was determined as the intersection point between the energy axis at the absorption offset and the line extrapolated from the linear portion of the absorption edge in the α/S vs E (eV) plot.

Results and Discussion

Structure of A₂BaCu₈Te₁₀. The structure type of A₂BaCu₈Te₁₀, the details of which have been described elsewhere,⁴ is two-dimensional with slabs of [BaCu₈Te₁₀]²⁻ separated by layers of A⁺ alkali metal cations; see Figure 1. The Cs salt on which the electronic structure calculation was made is orthorhombic *Immm* with $a = 7.109(1)$ Å, $b = 23.761(2)$ Å, and $c = 6.966(1)$ Å. Depending on the identity of the alkali metal ion, the structure can adopt either a monoclinic or an orthorhombic cell, the difference between the two being the stacking of the [BaCu₈Te₁₀]²⁻ layers. A strikingly characteristic feature in the structure is the Cu₈Te₁₂ pentagonal dodecahedral cage, which incarcerates the Ba²⁺ ions; see Figure 2. Each cage cluster contains three mutually perpendicular sets of ditelluride units. The Cu₈Te₁₂ cages form layers parallel to the (100) plane by sharing two pairs of oppositely spaced ditellurides along the *b*- and *c*-axis, respectively. The third and unshared Te₂²⁻ pair lines the surface of the Cu₈Te₁₀ layer. The geometry around the Cu atom is slightly distorted tetrahedral. Overall, the cage appears to have a strong affinity for cations with high charge/radius ratio, and so, given a choice between a Rb⁺ and a Ba²⁺ cation, it will encapsulate the latter. This preference is

(8) (a) Wendlandt, W. W.; Hecht, H. G. *Reflectance Spectroscopy*; Interscience Publishers: New York, 1966. (b) Kotüm, G. *Reflectance Spectroscopy*; Springer-Verlag: New York, 1969. (c) Tandon, S. P.; Gupta, J. P. *Phys. Status Solidi* **1970**, *38*, 363.

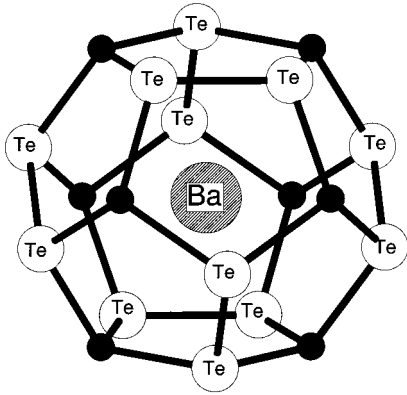


Figure 2. Ba-filled $\text{Cu}_8\text{Te}_{12}$ cage of $\text{Rb}_2\text{BaCu}_8\text{Te}_{10}$.

probably electrostatic in origin as the anionic layers of $[\text{Cu}_8\text{Te}_{10}]^{n-}$ attempt to reduce their negative charge. The bond distances between Cu and the Te_2^{2-} ligands range from 2.576(5) to 2.684(5) Å with an average of 2.64(5) Å. The Te–Te distances of the three ditellurides are in the range of 2.784(4) – 2.828(4) Å with an average of 2.80(2) Å. The Ba–Te distances inside the cage are almost independent of A^+ and average 3.75 Å. The corresponding shortest $\text{A}^+ - \text{Te}$ distances are 3.729(2) and 3.825(2) Å for Rb and Cs, respectively.

Interestingly, the Ba^{2+} ions do not have the largest ADPs in the crystal ($B_{\text{eq}} \sim 0.9$ vs average B_{eq} of 1.1 for remaining atoms) which suggests that hardly any Ba^{2+} ion “rattling” motion is present inside the $\text{Cu}_8\text{Te}_{12}$ cage. On the contrary, the largest ADPs are found in the Rb^+ atoms ($B_{\text{eq}} \sim 4.1$). It is these atoms that may be engaging in a rattling-like motion in their local environment. If so, how does this property affect the thermal conductivity in these materials?

Electronic Structure Calculations. Unlike the $\text{A}_3\text{Cu}_8\text{Te}_{10}$ compounds, which possess mixed-valency and are good p-type metals,⁴ the $\text{A}_2\text{BaCu}_8\text{Te}_{10}$ compounds are electron-precise, as replacement of Ba^{2+} for an alkali metal ion provides an additional electron to fill the hole in the valence band. As a result, they are expected to be semiconductors. However, given the diffuse nature of the Te s and p orbitals, any band gap may be exceedingly small. To gain better insight into the nature of the band gap, we performed electronic structure calculations at the DFT level of theory.

First principles calculations based on the local density approximation were used to determine the band structure, Raman phonon frequencies, and internal structural parameters of $\text{Cs}_2\text{BaCu}_8\text{Te}_{10}$. Electronic structure calculations were also performed for the barium-free analogue, $\text{Cs}_3\text{Cu}_8\text{Te}_{10}$, which is a metal.⁴ For $\text{Cs}_3\text{Cu}_8\text{Te}_{10}$, the experimental crystal structure was employed. The calculations for both compounds were done using the general potential linearized augmented plane-wave method (LAPW)⁹ with the Hedin–Lundqvist exchange-correlation function. This method uses a flexible basis and makes no shape approximations to either the potential or charge density. As such, it is well suited for open crystal structures with low site symmetry such as those under consideration here. Local orbital extensions to the basis¹⁰ were used to treat high lying core

Table 1. Internal Structural Coordinates of $\text{Cs}_2\text{BaCu}_8\text{Te}_{10}$ Determined from First Principles Total Energy Minimization

	<i>x</i>	<i>y</i>	<i>z</i>
Cs	0.5	0.0	0.223
Ba	0.5	0.5	0.0
Te(1)	0.5	0.0	0.061
Te(2)	0.0	0.286	0.0
Te(3)	0.298	0.5	0.139
Te(4)	0.0	0.0	0.163
Cu	0.191	0.192	0.090

Table 2. Calculated A_g Symmetry Raman Active Phonons from First Principles Calculations

freq (cm^{-1})	polarization	main character
128	<i>x</i>	Cu
169	<i>x</i>	Te(3)
131	<i>y</i>	Te(2)
187	<i>y</i>	Cu
56	<i>z</i>	Cs, Te(3) (rattling mode)
69	<i>z</i>	Cs, Te(3) (rattling mode)
123	<i>z</i>	Te(4)
150	<i>z</i>	Te(1), Te(3), Te(4), Cu
171	<i>z</i>	Te(1), Cu

states and to relax linearization generally. Well-converged basis sets consisting of approximately 4400 basis functions were used, along with a zone sampling consisting of 5 special *k*-points in the irreducible wedge for self-consistent iterations, and 59 uniformly distributed points in the wedge were used for the electronic density of states (DOS). LAPW sphere radii of 2.30 au were used for all atoms except Cu for which a 2.2 au radii was employed. Relativistic effects including spin-orbit were included in the calculation of the band structures and DOS. Lattice parameters were fixed at the experimentally determined values.

The crystal structure has nine independent internal coordinates corresponding to the *z*-axis Cs position, the *x*-, *y*-, and *z*-axis Cu positions, the *z*-axis positions of Te(1) and Te(4), the *y*-axis position of Te(2), and the *x*- and *z*-axis Te(3) positions. These were determined via total energy minimization using calculated atomic forces. The coordinates are given in Table 1 and remain remarkably close to the experimentally determined values. The Raman frequencies corresponding to these coordinates were determined by diagonalizing the dynamical matrix constructed from the calculated variation of the atomic forces. These are given in Table 2. It is noteworthy that the lowest lying modes (softest) are those associated with the Cs^+ atoms and they are expected at 56 and 69 cm^{-1} ; see Table 2. The low-frequency, mixed character of these modes is consistent with the “rattling” ion scenario for obtaining glasslike thermal conductivity.³ Unfortunately, we were unable to probe Raman frequencies below 90 cm^{-1} with our experimental apparatus.¹¹ Perhaps quasi-elastic neutron scattering could be of help here to observe and identify these very soft modes.¹²

The calculated DOS and projections on Cu and Te LAPW spheres for $\text{Cs}_2\text{BaCu}_8\text{Te}_{10}$ are shown in Figure

(10) Singh, D. J. *Phys. Rev. B* **1991**, *43*, 6388.

(11) We observe that the frequency Raman shifts for both $\text{Rb}_2\text{BaCu}_8\text{Te}_{10}$ and $\text{Cs}_2\text{BaCu}_8\text{Te}_{10}$ are almost identical and they occur at 123 cm^{-1} (strong), 140 cm^{-1} (medium), and 155 cm^{-1} (weak, shoulder), which are in reasonable agreement with theory; see Table 2. The 123 cm^{-1} frequency is likely to have its origin in the Te–Te vibration. Nevertheless, despite our inability to experimentally observe the “rattling” modes, the presence of soft phonon modes in this structure justified our expectations for low thermal conductivity in these materials.

(9) Singh, D. J. *Planewaves, Pseudopotentials and the LAPW Method*; Kluwer Academic Press: Boston, MA, 1994.

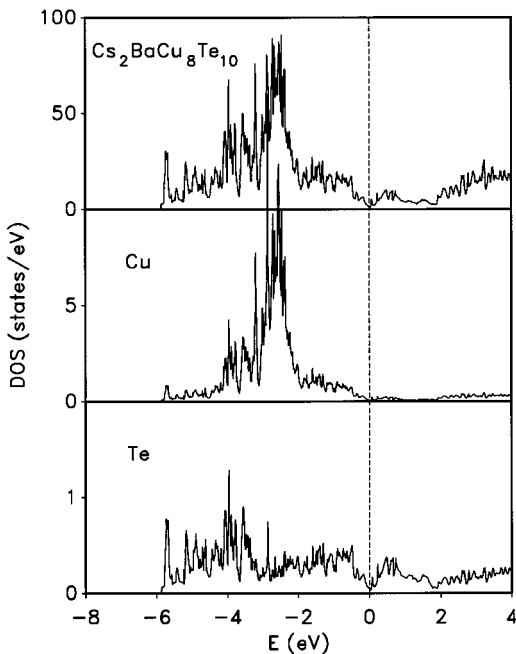


Figure 3. Electronic DOS of Cs₂BaCu₈Te₁₀ on a per formula unit basis and Cu and average Te projections on a per atom basis. E_F is at 0 eV and is denoted by the dashed vertical line.

3. The DOS of Cs₃Cu₈Te₁₀ is practically identical, apart from a shift of E_F , corresponding to the lower electron count, and is not shown. Ba and Cs are fully ionized and electronically inactive near the Fermi energy, E_F . Their role is essentially to provide charge and space filling. The main Cu 3d bands are narrow and located between -2.0 and -4.0 eV relative to E_F . However, hybridization with Te p states is evident, so that there is significant Cu d character extending from -5 eV to E_F . The electronic states above E_F are primarily Te-derived p orbitals, while those immediately below E_F are more hybridized mixtures of Te p and Cu d states. The Fermi level is seen to fall in a deep pseudogap. However, strictly speaking, the material may have to be characterized as a semimetal rather than a semiconductor, since the gap is not completely empty. The narrow-gap semiconductor versus semimetal characterization is hard to address unequivocally at this stage because we are pushing against the accuracy limits of our computational technique. It is well-known that the DFT methods tend to underestimate the band gaps of narrow gap semiconductors. Therefore experimental work was performed to resolve this issue; see below.

The band structure along selected symmetry directions is shown in Figure 4. Assuming that a very small gap actually exists, it is evident from Figure 4 that it is indirect. The top of the valence band occurs at the Γ and Z points ($\langle 100 \rangle$ direction), whereas the bottom of the conduction band occurs in several places in the Brillouin zone away from the zone boundaries. There are two optical thresholds expected from the band structure. The first involves transitions between the lower and upper band edges from the anti-crossing states; the second is the gap at the Z point, calculated as 0.20 eV.

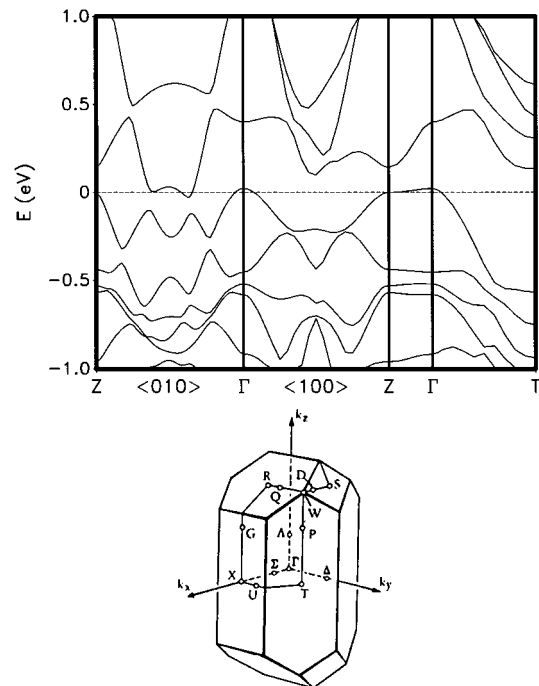


Figure 4. (top) Band structure of Cs₂BaCu₈Te₁₀ along selected directions in the body centered orthorhombic Brillouin zone. E_F is denoted by the dashed horizontal line at 0 eV. Note the hole cylinder along the c -axis Γ -Z line and the compensating electron pockets along the basal plane Γ -Z $\langle 010 \rangle$ direction. The estimation of very small energy gaps with the current method of calculation is not reliable. The top panel shows the valence band structure, while the bottom panel is a blowup of the region around E_F relevant to transport. (bottom) First Brillouin zone for body-center orthorhombic symmetry.

The hole cylinder around Γ is derived from well hybridized Te p and Cu d states and may be expected to have reasonable carrier mobility for transport in the ab -crystallographic plane. There is very little dispersion along the c -axis (Z) direction, and so this component of the resistivity should be much higher. In fact c -axis transport may well be incoherent at room temperature. The effective mass tensor of the whole cylinder at Γ has x - and y -components of 0.78 and 0.41 m_e , respectively. This implies significant anisotropy of the transport properties in the ab -plane as well. In the simplest, constant scattering kinetic transport theory, the b -axis conductivity of p-type samples, where this band dominates, would be 3.6 times larger than in the a -axis direction.¹³ This is the direction of the Te₂²⁻ bonds which cover both sides of the [BaCu₈Te₁₀] layers.

The electron states (n-type doping) derive from a band dominated by Te p orbitals, which dips down toward E_F at the nominal simple orthorhombic zone boundary. This corresponds to the midpoints of the basal plane $\langle 010 \rangle$ and $\langle 100 \rangle$ Γ -Z directions in the body-centered zone as shown in Figure 4. Along $\langle 100 \rangle$ this band just "kisses" E_F , while along $\langle 010 \rangle$ the dispersion is slightly larger so that it crosses E_F descending to -0.3 eV. However, there is an anticrossing with a hybridized band dispersing upward from Γ along this line to 0.05 eV above E_F at the midpoint (nominal zone boundary). The anticrossing opens a gap around E_F and mixes the

(12) Prassides, K.; Patschke, R.; Kanatzidis, M. G. Unpublished results.

(13) Kittel, C. *Introduction to Solid State Physics*, 6th ed.; John Wiley & Sons: New York, 1986; p 150.

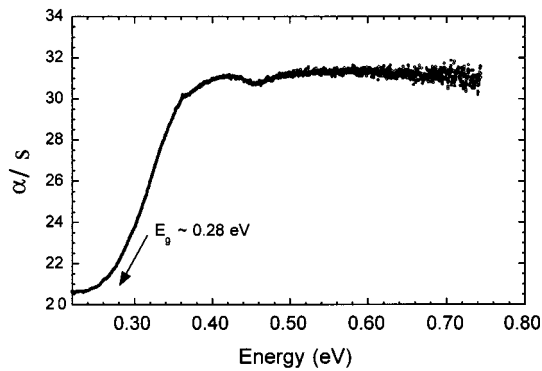


Figure 5. Infrared absorption spectrum of $\text{Rb}_2\text{BaCu}_8\text{Te}_{10}$ taken in diffuse reflectance mode.

character of these two bands. The resulting electron pockets have a complex shape and, like the hole cylinder, are considerably less dispersive in the c -axis direction as compared with the ab -plane.

We note that the band structure of the isostructural $\text{Cs}_3\text{Cu}_8\text{Te}_{10}$ around E_F is very similar and shows the same features, except that the electron count is reduced by one, so that E_F lies below rather than above the gap produced by the anticrossing. The main difference around E_F is an upward shift of a little more than 0.2 eV of the anticrossing relative to the band comprising the hole cylinder. This rigid band property has implications for the charge transport. In particular, it suggests that Cs impurities on the Ba^{2+} site of $\text{Cs}_2\text{BaCu}_8\text{Te}_{10}$ should be effective p-type dopants providing carriers but with little scattering. Also, soft phonons that may be associated with A^+ (Rb, Cs) atom vibrations will show moderately weak electron-phonon interactions, implying low thermal conductivity but reasonably high hole mobility in these materials.

Energy Gap. Experimental efforts were made to assess the band gap by optical absorption spectroscopy as well as magnetic susceptibility and heat capacity measurements. The last two techniques explore the density of states at the Fermi level; they do not directly measure the size of the energy gap. Lack of such states is consistent with the presence of a gap.

Absorption spectroscopy measurements in the mid-IR region ($4000\text{--}600\text{ cm}^{-1}$) are reliable in obtaining the energy gaps of narrow gap semiconductors. An electronic absorption is observed at $\sim 0.28\text{ eV}$ which can be assigned to a band gap; see Figure 5.

Magnetic susceptibility measurements on $\text{A}_2\text{BaCu}_8\text{Te}_{10}$ ($A = \text{Rb, Cs}$) show the compounds to be diamagnetic ($\chi_D = -0.00027\text{ emu/mol}$) consistent with the lack of appreciable DOS at the Fermi level and consequent semiconducting behavior. The susceptibility remains negative over the full temperature range; see Figure 6. Below 10 K paramagnetic impurities begin to be observed.

Heat Capacity of $\text{Rb}_2\text{BaCu}_8\text{Te}_{10}$. To address the question of whether there is an energy gap at E_F in these compounds, we measured the heat capacity as a function of temperature in the range of 2 to 300 K. The heat capacity of solids at constant pressure is typically given by the relationship

$$C_p = \gamma T + \beta T^3$$

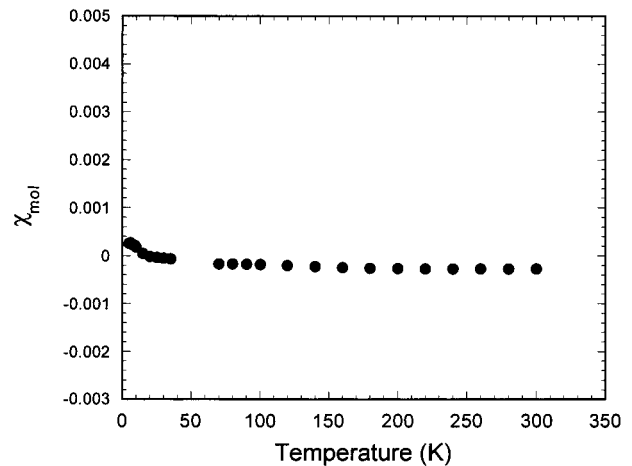


Figure 6. Magnetic susceptibility of $\text{Rb}_2\text{BaCu}_8\text{Te}_{10}$ as a function of temperature. The susceptibility crosses into positive territory at $<20\text{ K}$ due to the effects of paramagnetic impurities.

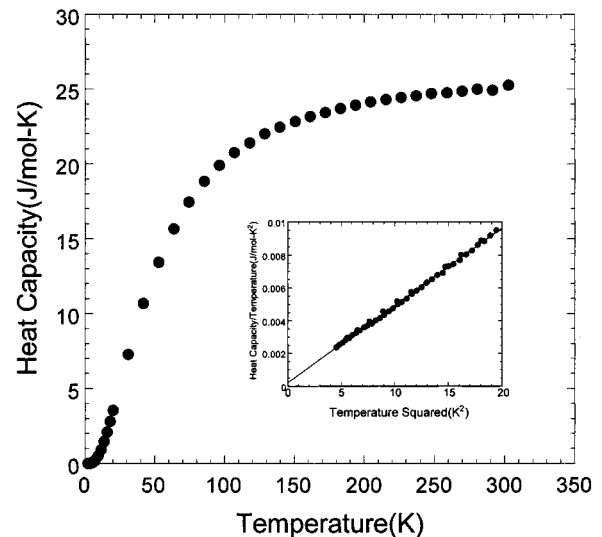


Figure 7. Heat capacity of $\text{Rb}_2\text{BaCu}_8\text{Te}_{10}$ as a function of temperature. Inset: Low-temperature data plotted as C_p/T vs T^2 .

where the first term, γT , is the electronic contribution to the heat capacity and the second term, βT^3 , is the lattice contribution to the heat capacity. The parameters γ and β are related to the electron density and Debye temperature, Θ_D , as will be discussed shortly. This relationship holds for simple materials which do not exhibit any magnetic, structural, or electronic phase transitions that can obscure or contribute to the heat capacity. Semiconductors with a well-defined energy gap have $\gamma = 0$. Heat capacity data obtained over a wide range of temperatures are shown in Figure 7.

Important information such as $N(0)$, the electronic density of states at the Fermi energy at $T \rightarrow 0$ and the Θ_D can be obtained from the following relationships extracted from the low-temperature heat capacity data:

$$N(0) = 0.4244\gamma/(1 + \lambda)$$

$$\Theta_D = 10(1.944/\beta)^{1/3}$$

where λ is the coupling strength of the electrons to both the lattice vibrations (phonons) and to other electrons.

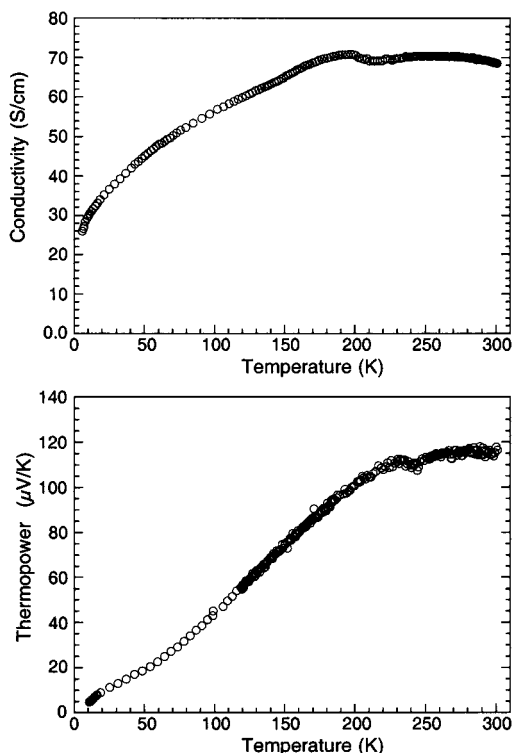


Figure 8. Variable-temperature single-crystal electrical conductivity data (top) and thermopower data (bottom) for K₂BaCu₈Te₁₀.

Θ_D indicates the temperature of the highest frequency phonon modes and therefore provides an indication as to the stiffness of the interatomic force constants and bonding energies. One can therefore expect the lattice thermal conductivity of simple, nonmetallic solids to scale as Θ_D .¹⁴ We point out, however, that the compounds discussed in this paper may not be “simple solids”. Their crystal structures and compositions are complex; they have low symmetry and are composed of relatively “stiff” parts (e.g. [BaCu₈Te₁₀]) and “soft” parts such as the interlayer regions where the alkali metals reside. From our low-temperature heat capacity measurements the estimated Θ_D for the Rb₂BaCu₈Te₁₀ and Cs₂BaCu₈Te₁₀ samples are about 350 and 315 K, respectively.

Application of a magnetic field had no effect on the temperature dependence or the magnitude of the heat capacity. The γ values for both compounds derived from the low-temperature data, see inset of Figure 7, average 0.28 mJ/(mol K²). Typical metals have γ values from 0.008 to 10.7 mJ/(mol K²). However, there are examples of semiconductors that have γ only slightly > 0 within the range observed here.¹⁵ The deviation from zero can be explained by the presence of impurities making the material a degenerate semiconductor. Therefore, we can conclude that the A₂BaCu₈Te₁₀ (A = Rb, Cs) materials are narrow gap semiconductors. The negative band gap suggested by the band structure calculations seems to be an artifact of the method used as such calculations generally underestimate band gaps.

(14) In fact $\kappa_1 \propto \Theta_D^3$; see, for example: Berman, R. *Thermal Conductivity in Solids*; Clarendon Press: Oxford, U.K., 1976.

(15) Kittel, C. *Introduction to Solid State Physics*, 6th ed.; John Wiley & Sons: New York, 1986; pp 141 and 413–416.

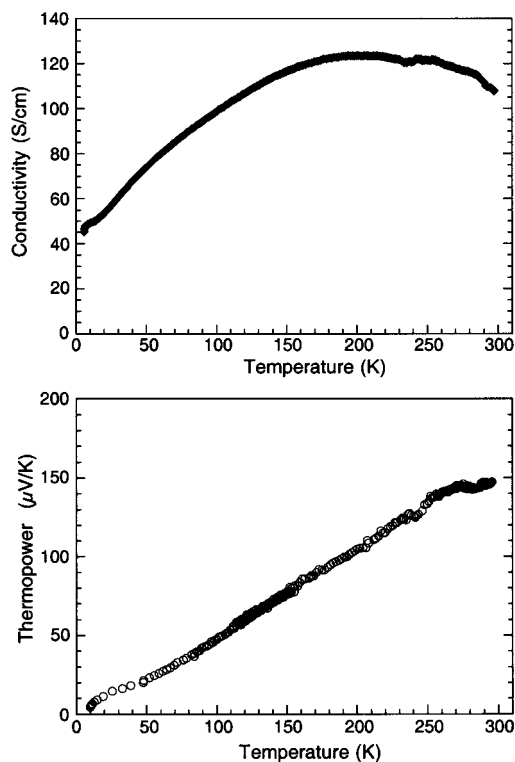


Figure 9. Variable-temperature single-crystal electrical conductivity data (top) and thermopower data (bottom) for Rb₂BaCu₈Te₁₀.

Electronic Transport Properties. The electrical charge transport behavior in A₂BaCu₈Te₁₀ seems to vary depending on the sample preparation conditions. Both semiconducting samples with relatively low electrical conductivity and metallic-like samples can be obtained. Samples obtained from Ba-rich conditions tend to show a thermally activated dependence of the conductivity. Such synthetic conditions can be established either in the polychalcogenide flux¹⁶ or by deliberately adding excess Ba or BaTe in the syntheses described in this paper. If such excess is not added, the samples tend to have almost metallic conductivity as they become degenerately doped.

Electronic transport measurements on single crystals of K₂BaCu₈Te₁₀ and Rb₂BaCu₈Te₁₀ (prepared in flux) confirm the semiconducting/semimetallic nature. The electrical conductivity and thermoelectric power data are shown in Figures 8 and 9. The sign and magnitude of the Seebeck coefficients of K₂BaCu₈Te₁₀ and Rb₂BaCu₈Te₁₀ suggest p-type semiconductors. The holes are delocalized on primarily Te-based p orbitals. The electrical conductivities of both K₂BaCu₈Te₁₀ and Rb₂BaCu₈Te₁₀ rise with increasing temperature but become flat or reach a maximum at or above 200 K.

Samples prepared by a direct combination reaction are polycrystalline ingots and tend to come highly doped (unless the Ba concentration is in great excess). For example, Figure 10 shows a set of electrical conductivity and thermoelectric power data obtained from polycrystalline ingots of Rb₂BaCu₈Te₁₀. Notice that the magnitude of the electrical conductivity is larger at ~ 550 S/cm, the maximum observed in the single crystals has

(16) Kanatzidis, M. G.; Sutorik, A. C. *Prog. Inorg. Chem.* **1995**, *43*, 151.

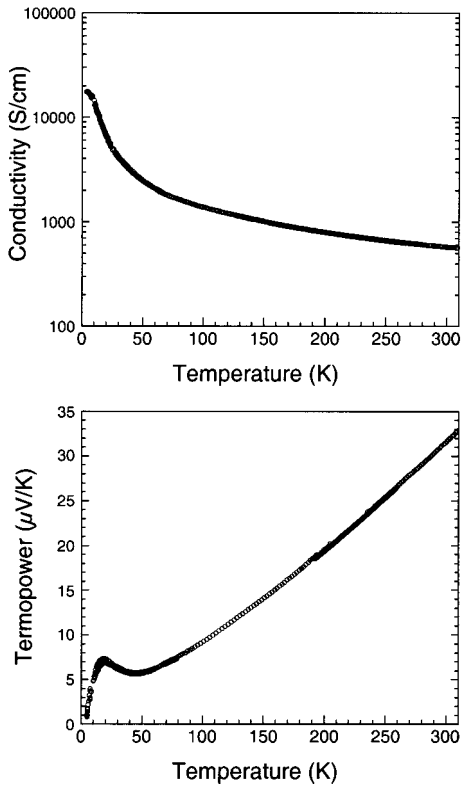


Figure 10. Variable-temperature electrical conductivity and thermopower data for a polycrystalline ingot of $\text{Rb}_2\text{BaCu}_8\text{Te}_{10}$.

disappeared, and the conductivity has increased dramatically. The Seebeck coefficient has dropped to small values of $\sim +34 \mu\text{V}/\text{K}$, indicating many more carriers in these samples, i.e., degenerate doping levels in this material. The thermopower appears to have a small low-temperature phonon drag peak at approximately $T \sim 20 \text{ K}$. The differences between the flux-grown single-crystal samples and the polycrystalline ingots reflect differences in the doping level.

Small deviations from stoichiometry of the type $\text{K}_2(\text{Ba}_{1-x}\text{K}_x)\text{Cu}_8\text{Te}_{10}$ are a mechanism to introduce holes in the valence band of the Cu–Te framework and dramatically alter the charge transport properties of the material from a semiconductor to a metal. Figure 11 shows the charge transport properties of such a sample that exhibits an order of magnitude higher conductivity and greatly reduced positive thermopower, characteristic of metals. The slight excess of K^+ ions was determined by microprobe energy dispersive spectroscopy (EDS) analysis and corresponds to $x \sim 0.1$. The $\text{A}_2(\text{Ba}_{1-x}\text{A}_x)\text{Cu}_8\text{Te}_{10}$ system can support the full range of x values from 0 to 1 as the $x = 1$ compounds (i.e. $\text{A}_2(\text{A}_1)\text{Cu}_8\text{Te}_{10}$) have metallic properties.⁴ This type of “doping” may be one way to optimize the thermoelectric properties of these materials.

Thermal Conductivity. Figure 12 shows the thermal conductivity of polycrystalline $\text{Cs}_2\text{BaCu}_8\text{Te}_{10}$ and $\text{Rb}_2\text{BaCu}_8\text{Te}_{10}$ measured as a function of temperature. The data indicate a rather low value at room temperature of $\sim 14 \text{ mW}/\text{cm}\cdot\text{K}$, lower than that of Bi_2Te_3 ($\kappa_{\text{L}} \sim 17 \text{ mW}/\text{cm}\cdot\text{K}$).¹⁷ Using the measured values of the

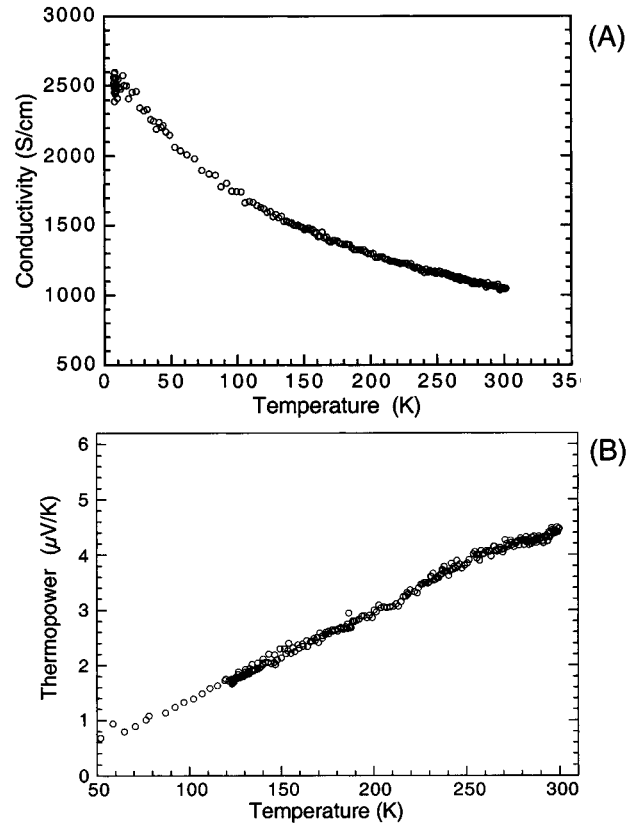


Figure 11. Variable-temperature single-crystal electrical conductivity data (A) and thermopower data (B) for $\text{K}_{2+x}\text{Ba}_{1-x}\text{Cu}_8\text{Te}_{10}$ ($x = 0.1$). Current flow was along the slabs.

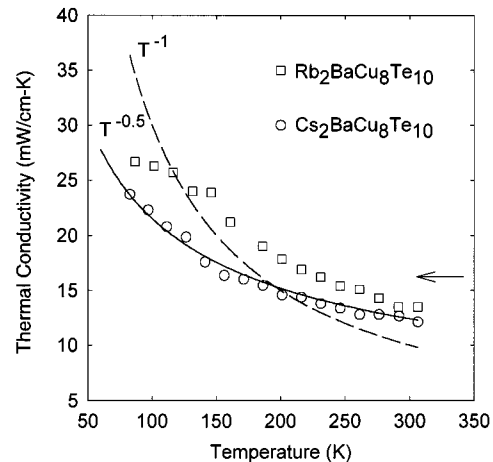


Figure 12. Variable-temperature thermal conductivity data for polycrystalline $\text{Cs}_2\text{BaCu}_8\text{Te}_{10}$ and $\text{Rb}_2\text{BaCu}_8\text{Te}_{10}$. Simple fits assuming predominantly phonon–phonon (T^{-1}) and alloy ($T^{-0.5}$) scattering are also shown. The arrow indicates the typical room-temperature lattice thermal conductivity value of optimized $\text{Bi}_2\text{Te}_{3-x}\text{Se}_x$ alloy parallel to the crystallographic c -axis.

electrical resistivity ($3.4 \text{ m}\Omega \text{ cm}$ at room temperature), in conjunction with the Wiedemann–Franz law,¹³ we estimate the maximum value of the electronic thermal conductivity contribution to be less than 20% of the total thermal conductivity of $\text{Rb}_2\text{BaCu}_8\text{Te}_{10}$. Thus, essentially all heat in the sample is carried by lattice phonons.

At room temperature, the thermal conductivity has a value close to that of vitreous silica.¹⁸ The thermal conductivity is lower in magnitude than most filled-

(17) *Encyclopedia of Materials Science and Engineering, Thermoelectric Semiconductors*; MIT Press and Pergamon Press: Cambridge, MA, Oxford, U.K., 1986.

skutterudite compounds, a class of materials with potential for thermoelectric applications.¹⁹ Hence, Rb₂BaCu₈Te₁₀ appears to possess a low enough thermal conductivity to make it worthy of further investigations aimed at improving its thermoelectric performance.

The question to be addressed here is this: is the very low thermal conductivity of these compounds due to the presence of "rattling" Rb⁺ ions in Slack's concept of a PGEC material or due to other contributing factors? To begin to understand this issue we fitted the data to a T^{-1} (phonon-phonon scattering) and to a $T^{-0.5}$ (alloy type scattering) temperature dependence; see Figure 12. If the "rattling" motion of the alkali metal atoms were primarily responsible for the low thermal conductivity, the rise in value with decreasing temperature should not be observed. From this simple analysis it appears that "rattle" scattering is not the major phonon scattering mechanism in these compounds. In fact, alloy scattering fits well the Cs₂BaCu₈Te₁₀ compound. The thermal conductivity data of the Rb analogue may possess some $T^{-0.5}$ temperature dependence while at low temperatures (<130 K) the data deviates downward with decreasing temperature from the $T^{-0.5}$ curve fit. This could be due to the contribution of some Rb atom rattling; however, more than one phonon scattering mechanism appears to be responsible for this temperature dependence. How does the alloy type scattering arise in the Cs₂BaCu₈Te₁₀ compound? We reason that Cs and Ba atoms may be more disordered in this compound than in the Rb analogue in which the crystallographic refinement indicated very little or no

disorder. Unfortunately, it was not possible to distinguish the Cs and Ba atoms in the structure of Cs₂BaCu₈Te₁₀ because Cs and Ba scatter X-rays almost identically. A neutron diffraction study will be needed to resolve this issue.

Concluding Remarks

The A₂BaCu₈Te₁₀ phases are narrow gap semiconductors with very low thermal conductivity. However, the heat conduction in these materials seems to be frustrated mainly by factors such as low crystal symmetry and possibly mass fluctuation disorder between alkali (i.e. Cs case) ions and Ba ions in the structure and less by soft rattling modes of the alkali A⁺ atoms between the layers. The moderately high room-temperature conductivity of these compounds, coupled with their relatively high thermopower values and very low thermal conductivity, raises the possibility that they may be valuable for thermoelectric applications if additional optimization were possible. One way to improve the properties is by tuning the energy gap through appropriate elemental substitutions (e.g. Se for Te) in the structure as well as the possibility to generate both p-type and n-type samples.

Acknowledgment. Financial support from the Office of Naval Research and DARPA is gratefully acknowledged. The work made use of the SEM facilities of the Center for Electron Optics at Michigan State University. At NU this work made use of Central Facilities supported by NSF through the Materials Research Center (Grant DMR-96-32472).

CM0003900

(18) Cahill, D. G.; Watson S. K.; Pohl, R. O. *Phys. Rev. B* **1992**, *46*, 6131.

(19) Nolas, G. S.; Morelli, D. T.; Tritt, T. M. *Annu. Rev. Mater. Sci.* **1999**, *29*, 89-116.